Proceedings of the Thirty-fifth (2025) International Ocean and Polar Engineering Conference **www.isope.org**
Seoul/Goyang, Korea, June 1-6, 2025

ISBN 978-1-880653-74-6; ISSN 1098-6189

Super-Resolution Reconstruction of Incompressible Turbulent Channel Flows with Global Pressure Correlation

Maokun Ye[1], *Jie Zhu*[2], *Guohua Pan*[3], *Decheng Wan*[1*]

[1] Computational Marine Hydrodynamics Lab (CMHL), School of Naval Architecture, Ocean and Civil Engineering, Shanghai Jiao Tong University, Shanghai, China
[2] Wuhan Second Ship Design and Research Institute, Wuhan, China
[3] Ningbo Pilot Station, Ningbo Dagang Pilotage Co., Ltd., Ningbo, China

*Corresponding Author

ABSTRACT

Turbulent flows, especially at high Reynolds numbers are resource-demanding to resolve using numerical simulations. Due to the multi-scale nature of fully turbulent flows, the spatial resolution in an LES calculation needs to be extremely high, and this results in a formidable number of computational grids, e.g., to the order of 100 million. Therefore, to obtain high-resolution flow field from low-resolution flow data is of great practical interest for turbulent flow predictions. This paper proposed a data-driven modeling framework for super-resolution (SR) reconstruction of turbulent channel flow from low-resolution flow field, in which the elliptic nature of the mass-conservation in incompressible fluids is leveraged to enhance the performance of neural networks. Specifically, inspired by the attention mechanism which is frequently adopted in natural language processing or time series analysis to capture global correlations among variables, we input pressure data obtained from globally distributed sensors as additional features to infer the local flow quantities, i.e. three instantaneous velocity components. By adopting this strategy, the global correlations among different spatial points are readily taken into account. This work first introduces the generation of high-fidelity training data set by using LES calculations, and the low-resolution flow field is obtained from the high-fidelity field by applying spatial filters. Then, a neural network mapping relation from the low-resolution flow field to the high-resolution flow field is established. Finally, the reconstructed flow fields are visualized and discussed.

KEY WORDS: Super-Resolution Reconstruction; Machine Learning; Turbulent Flow.

INTRODUCTION

Turbulent flow is ubiquitous in ocean engineering applications, yet resolving it poses significant challenges due to its inherently multi-scale nature in both time and space. In Large Eddy Simulations (LES) of high Reynolds number flows, the total number of computational points can easily exceed 100 million, often leading to prohibitively high computational costs. However, with the rapid advancement of machine-learning technology, there is growing optimism about its potential to revolutionize the modeling and simulation of turbulent flows, offering more efficient while reliable solutions. For instance, Fukami et al. (Fukami et al., 2019) pioneered a CNN-based approach to connect low-resolution images to high-resolution ones, initially applying it to two-dimensional cylinder wake flows, both turbulent and laminar, as well as two-dimensional homogeneous decaying turbulence. This framework was later extended to achieve super-resolution reconstruction of turbulent flow fields in both space and time (Fukami et al., 2020). Building on this, Liu et al. (Liu et al., 2020) enhanced the accuracy of neural network predictions by incorporating temporal dependencies through multiple temporal paths. Further advancements were made by Bi et al. (Bi et al., 2022), who integrated an attention mechanism into CNN-based SRCNN networks to more efficiently capture global spatial correlations in turbulent flows, achieving significant improvements in performance.

The core idea behind these studies is to train neural network models to take low-resolution flow fields as input and output high-resolution results. This approach allows high-resolution flow fields to be obtained by performing CFD simulations on coarser grids, thereby significantly reducing computational resource requirements. However, the aforementioned studies all adopted pure data-driven framework, i.e., when training the neural network models, the “flow field” was treated as “image”. The super-resolution of the flow field is more or less a pure image-processing problem., and limited, or little, physical knowledge of the flow field was incorporated in the modeling process.

In recent years, researchers have increasingly focused on integrating more prior physical into the modeling of artificial neural networks. This approach aims to enhance the accuracy, interpretability, and generalizability of neural networks by embedding fundamental physical principles directly into the learning process. Specifically, incorporating physical knowledge into neural networks can be achieved at either the output or the input end of the model. The first approach, known as

Physics-Informed Neural Networks (PINNs) (Raissi et al., 2019), introduces physical constraints directly into the optimization process of the neural network. This ensures that the model's predictions adhere to fundamental physical laws. The second approach, often referred to as Physics-Guided Neural Networks (PGNNs) (Yousif et al., 2022; Li et al., 2024), involves feeding the neural network with lower-fidelity data as a guiding framework during training. This method leverages approximate physical models or data to steer the learning process, enhancing the model's ability to generalize and produce physically consistent results.

In this work, we propose a data-driven modeling framework based on PGNN for the SR reconstruction of turbulent channel flow from low-resolution flow fields. Our approach leverages the elliptic nature of pressure equation in incompressible flows to enhance the performance of the neural network. Inspired by the attention mechanism—commonly used in natural language processing and time series analysis to capture global correlations—we incorporate pressure data from globally distributed sensors as additional input features. This allows the model to infer local flow quantities, specifically the three instantaneous velocity components, while naturally accounting for global correlations across different spatial points. By integrating these strategies, our framework effectively combines physical principles with data-driven learning to improve the accuracy and robustness of super-resolution reconstruction in turbulent flows.

The remainder of this paper is organized as follows. First, we provide a detailed explanation of the generation of the high-fidelity dataset. Next, we introduce the neural network (NN) model used in this study, including its architecture, the mapping relationship it aims to establish, and the preparation of the training dataset. Subsequently, the NN model is trained and applied to the super-resolution reconstruction of fully developed turbulent flow, using lower-resolution data as input. Finally, conclusions are drawn based on the results and discussions presented.

GENERATION OF HIGH-FIDELITY DATASET

In machine learning tasks, a high-quality dataset is considered a fundamental prerequisite. Therefore, in this chapter, we will detail the process of generating the high-quality dataset used in this study.

CFD Approach

After applying a spatial filter to the incompressible N-S equations, the governing equations can be written as:

$$\frac{\partial \tilde{u}_i}{\partial x_i} = 0 \tag{1}$$

$$\frac{\partial \tilde{u}_i}{\partial t} + \frac{\partial \tilde{u}_i \partial \tilde{u}_j}{\partial x_j} = -\frac{1}{\rho} + \frac{\partial \tilde{p}}{\partial x_i} + \upsilon \frac{\partial^2 \tilde{u}_i}{\partial x_j \partial x_j} - \frac{\partial \tau_{ij}}{\partial x_j} \tag{2}$$

where $\tilde{u}_i (i = 1,2,3)$ is the filtered velocity component in the x_i direction. p is the filtered pressure, υ the kinematic viscosity of the fluid, and τ_{ij} is the so-called sub-grid stress which is given by

$$\tau_{ij} = \frac{2}{3} k_{sgs} \delta_{ij} - 2\upsilon_{sgs} \tilde{S}_{ij} \tag{3}$$

where $\tilde{S}_{ij}$ is the resolved strain-rate tensor, while υ_{sgs} being the unresolved eddy viscosity and need additional model to close. In the current work, the wall-adapting local eddy-viscosity (WALE) model (Nicoud and Ducros, 1999) is applied, and the unresolved eddy viscosity is written as:

$$\upsilon_{sgs} = (C_w \Delta)^2 \frac{\left(S_{ij}^d S_{ij}^d\right)^{3/2}}{\left(\tilde{S}_{ij} \tilde{S}_{ij}\right)^{5/2} + \left(S_{ij}^d S_{ij}^d\right)^{5/4}} \tag{4}$$

where $C_w = 0.325$ is the WALE coefficient, Δ is the cube root of local cell volume, S_{ij}^d is the traceless symmetric part of the square of the velocity gradient tensor which is defined by:

$$S_{ij}^d = \frac{1}{2}\left(\frac{\partial \tilde{u}_i \partial \tilde{u}_k}{\partial x_k \partial x_j} + \frac{\partial \tilde{u}_j \partial \tilde{u}_k}{\partial x_k \partial x_i}\right) - \frac{1}{3} \delta_{ij} \frac{\partial \tilde{u}_k \partial \tilde{u}_l}{\partial x_l \partial x_k} \tag{5}$$

Numerical Setup

Fig. 1 illustrates the computational domain used in the CFD simulations for this study. The domain dimensions are $L_x \times L_y \times L_z = 2\pi\delta \times 2\delta \times \pi\delta$, where δ represents the channel half-height. The coordinate system is defined as follows: x corresponds to the streamwise direction, y to the wall-normal direction, and z to the spanwise direction. Periodic boundary conditions are applied to the side walls, while the top and bottom walls are set as no-slip boundaries.

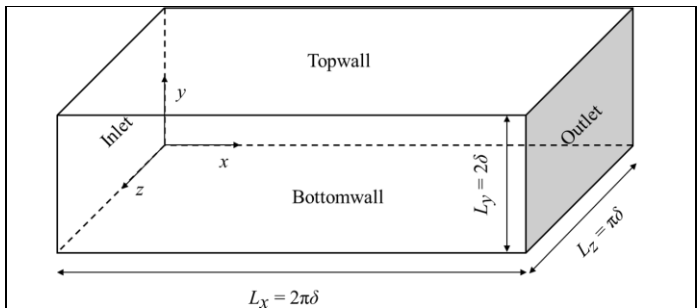

Figure 1. Illustration of the computational domain.

In this study, the Reynolds numbers are defined based on the bulk velocity and friction velocity. Specifically, the bulk Reynolds number is given by $Re_b = U_b\delta/\nu = 20000$, and the friction Reynolds number is $Re_\tau = u_\tau\delta/\nu = 1000$. Here, $u_\tau = \sqrt{\tau_w/\rho}$ represents the friction velocity at the wall, where τ_w is the wall shear stress and ρ is the fluid density.

The specifications of the computational grid are detailed in Table 1. The grid consists of 320 cells in the streamwise direction (x), 216 cells in the wall-normal direction (y), and 320 cells in the spanwise direction (z). This configuration results in a total of approximately 22 million grid points used in the CFD simulations.

Table 1. Computational grid specifications

Parameter	**Value**
Δx^+	19.6
Δy^+	0.79 ~ 15.0
Δz^+	9.8
$N_x \times N_y \times N_z$	320 × 216 × 320
N_{total}	22.1 million

CFD Results

The verification and validation of the CFD results have been extensively discussed in a previous paper by the authors and are therefore omitted here for brevity. Readers are encouraged to refer to our earlier work for detailed information. Within the scope of this paper, we focus on the flow snapshots from the LES dataset. As illustrated in Fig. 2, the velocity components (U, V, W) and the pressure field (p) on the central slice of the computational domain are presented, providing a clear visualization of the flow characteristics.

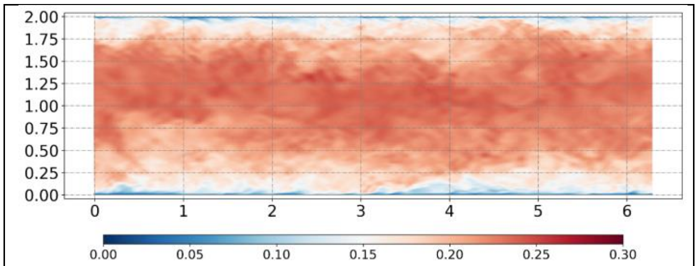

(a) U

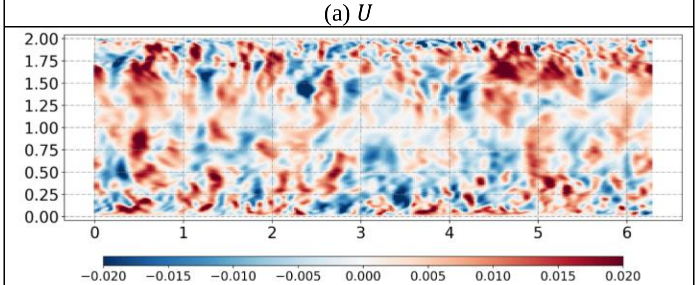

(b) V

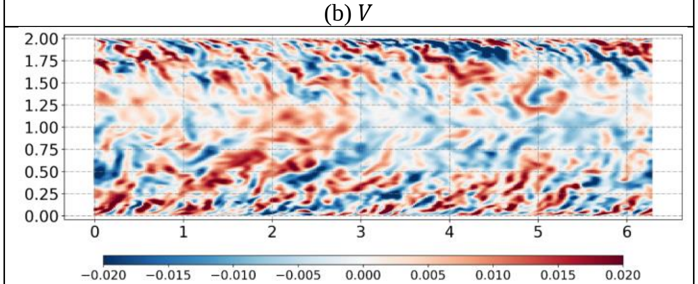

(c) W

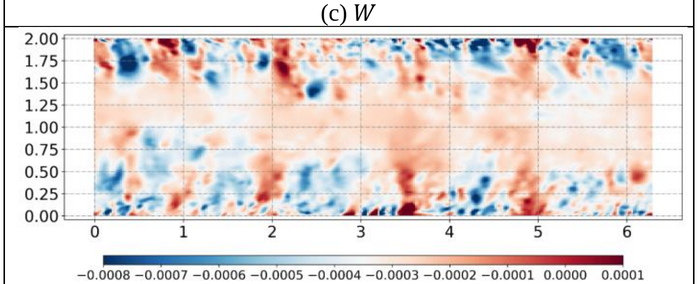

(d) p

Figure 2. LES results, i.e. the HR flow field.

DEFINITION OF ANN FOR THE SR RECONSTUCTION OF TURBULENT CHANNEL FLOW

Definition of ANN Structure

A Multilayer Perceptron (MLP) network is composed of an input layer, one or more hidden layers, and an output layer. The input layer receives the initial data, which is then propagated forward through the hidden layers to the output layer. Each hidden layer applies a series of non-linear transformations to the input, enabling the network to capture and model intricate relationships between the input and output data. In the present study, we employ this fundamental neural network structure for illustrative and demonstrative purposes. A visual representation of an MLP is provided in Fig. 3.

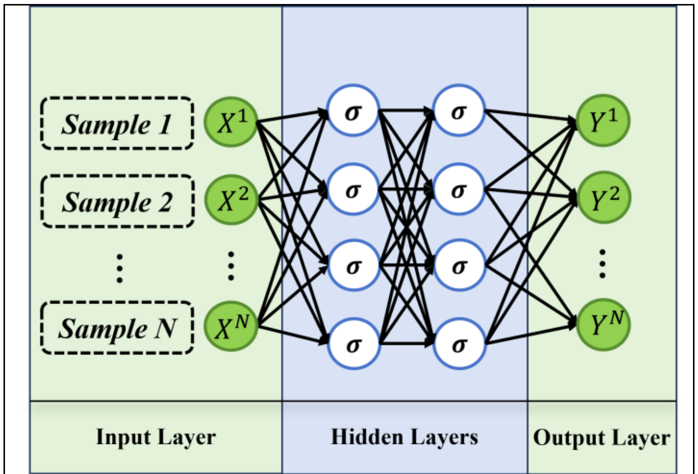

Figure 3. Illustration of an MLP.

Fig. 4 illustrates the detailed operations within a node of the hidden layers in an MLP. Each node in the hidden layer computes a weighted sum of its inputs, which is then passed through an activation function, denoted as σ in Fig. 2. This activation function introduces non-linearity, enabling the node to model complex patterns in the data. During the training process, the MLP network employs backpropagation to iteratively adjust the weights. Backpropagation calculates the gradient of the loss function with respect to the weights, allowing the network to optimize the weights in a way that minimizes the discrepancy between the predicted output and the true output. This iterative optimization process enables the network to learn the underlying relationships between the input and output data effectively.

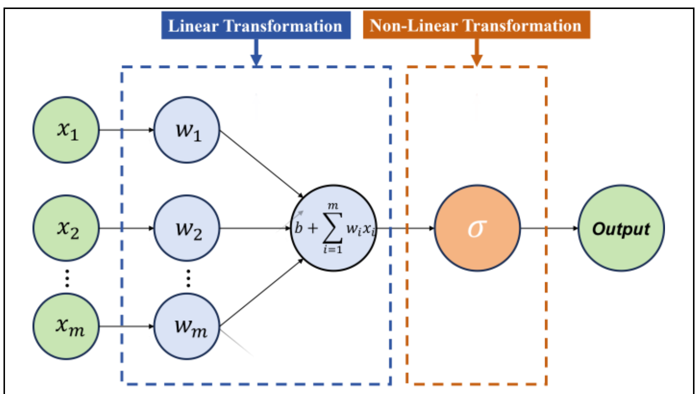

Figure 4. Illustration of an MLP node.

Definition of Mapping Relation

In this study, the mapping relationships to be established by the NN model are formulated in Eq. (6) and Eq. (7). Here, Eq. (6) serves as a benchmark for comparative analysis, providing a reference point to evaluate the performance of the proposed PGNN model, i.e. Eq. (7).

$$(U^{HR}, V^{HR}, W^{HR}, p^{HR}) = \boldsymbol{NN}(x, y, z) \quad (6)$$

$$(U^{HR}, V^{HR}, W^{HR}, p^{HR}) = \boldsymbol{PGNN}(x, y, z, p^{LR}) \tag{7}$$

Preparation of Training Dataset

The flow field depicted in Fig. 2 is initially down-sampled to generate LR data, which serves as the training data of the two NN models. In this study, a down-sampling ratio of 10 is applied to derive the LR data from the HR data. The resulting LR flow field data points are then utilized to train the NN models, as defined by Eqs. (6) and (7). The process of down-sampling the HR data is visually demonstrated in Fig. 5.

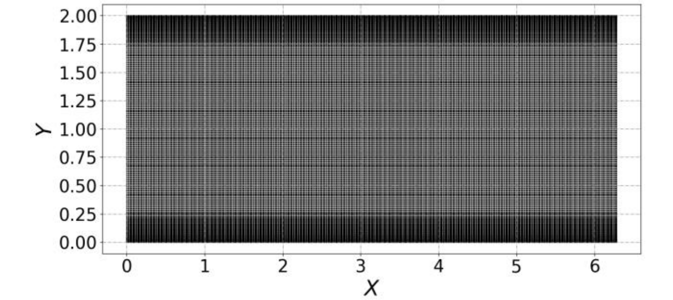

(a) data points of the HR data.

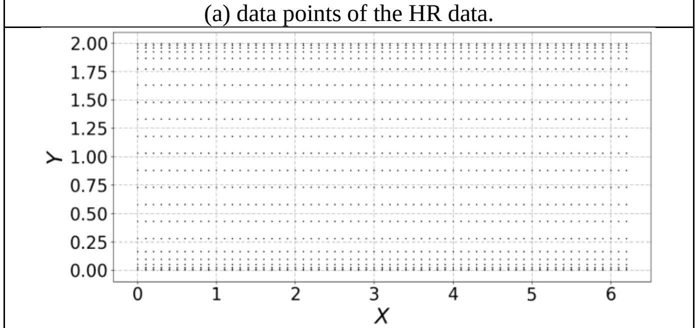

(a) data points of the LR data.

Figure 5. Down-sampling of the HR data.

The resulting down-sampled flow field, i.e., the LR flow field, which includes the three velocity components (*U*, *V*, *W*) and the pressure field (*p*), is illustrated in Fig. 6.

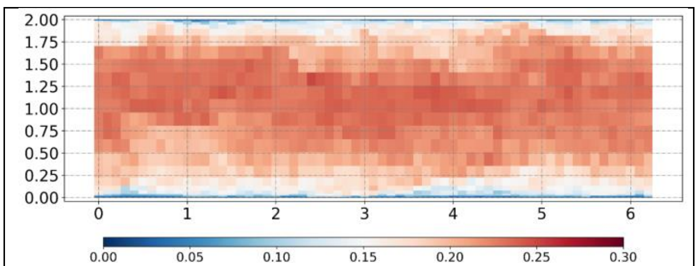

(a) U^{LR}

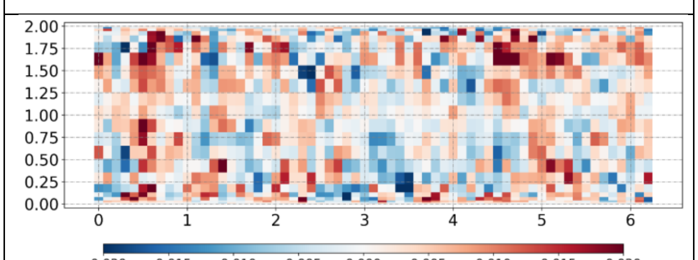

(b) V^{LR}

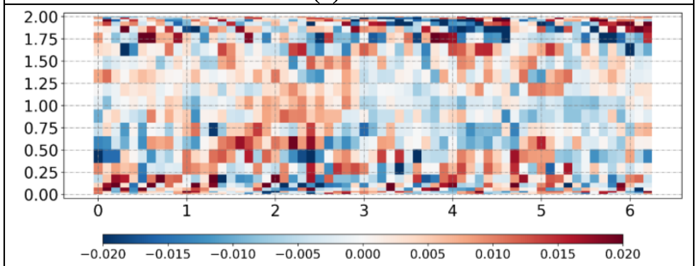

(c) W^{LR}

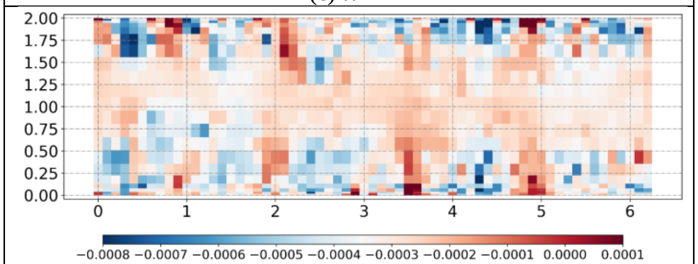

(d) p^{LR}

Figure 6. LR flow field.

The total number of training data points is around 8,000, and the data points of the LR flow field are then randomly split into a training dataset and a testing dataset in a ratio of 9:1. The data points in the training dataset are then utilized to train the two NN models.

RESULTS AND DISCUSSION

Training of the ANN Model

First, the training data points are randomly shuffled to ensure a balanced distribution. Next, min-max normalization is applied to standardize the original data, scaling all input features to the range [0, 1]. This normalization step helps enhance the training efficiency and performance of the neural network.

$$x_{normalized} = \frac{x - x_{min}}{x_{max} - x_{min}} \tag{8}$$

The hyperbolic tangent (tanh) function is employed as the activation function in the neural network model, defined as follows:

$$a_{tanh} = \frac{e^{x} - e^{-x}}{e^{x} + e^{-x}} \tag{9}$$

In the current study, the open-source deep-learning library PyTorch is used to construct and train the NN models. The constructed NN architecture consisted of 11 hidden layers with 100 neurons per layer. During the training process, the *Adamax* optimizer from PyTorch is utilized, and the batch size is 64, and the Mean Square Error (MSE) is used as the loss function with a learning rate of 0.0001.

The loss curve is illustrated in Fig. 7.

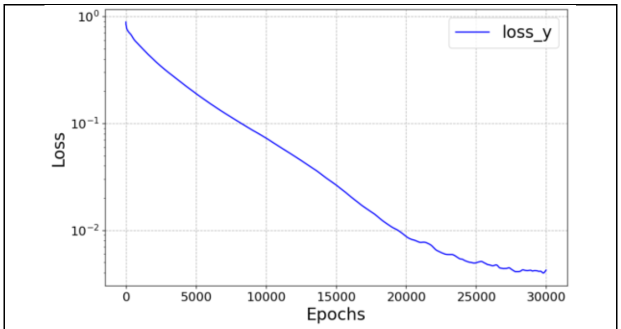

Fig.7 Histories of losses in the training process.

SR Construction of the Flow

After training with low-resolution flow field data, the two resulting NN models are used to reconstruct high-resolution flow fields, as shown in Figure 8. The left column displays the flow fields computed by CFD, which serve as the ground truth in this study. The middle column presents the results obtained from the neural network defined by Equation 7 (purely data-driven), while the right column shows the results from the neural network defined by Equation 8 (physics-guided).

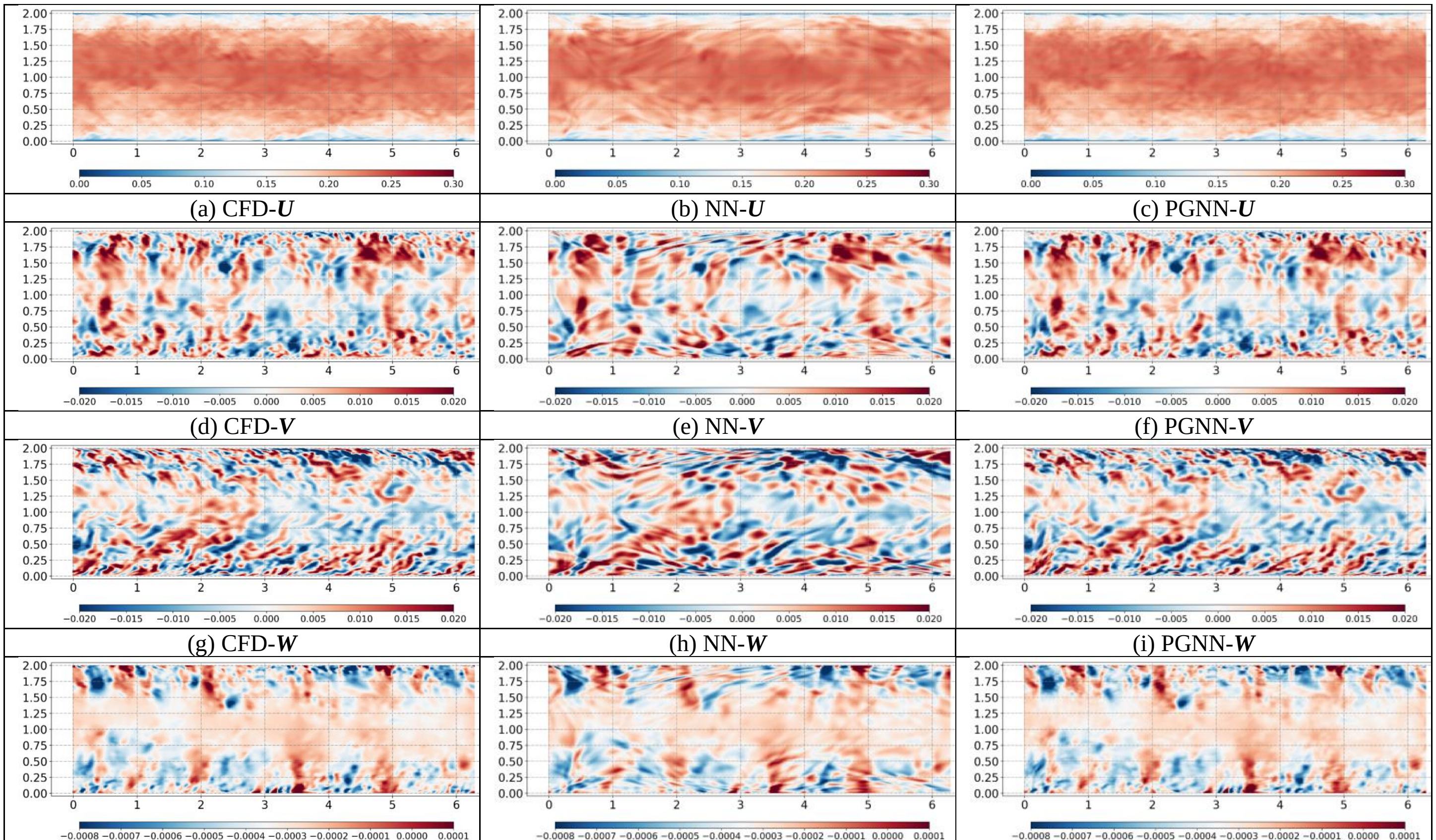

(a) CFD-***U*** (b) NN-***U*** (c) PGNN-***U***

(d) CFD-***V*** (e) NN-***V*** (f) PGNN-***V***

(g) CFD-***W*** (h) NN-***W*** (i) PGNN-***W***

(j) CFD-***p*** (k) NN-***p*** (l) PGNN-***p***

Figure 8. NN-reconstructed turbulent flow fields.

Comparing the reconstructed flow fields obtained from the pure data-driven model and the Physics-Guided Neural Network (PGNN), it is evident that the high-resolution flow field reconstructed by the PGNN is closer to the ground truth. Although the purely data-driven approach successfully captures the large-scale characteristics of turbulence, its accuracy in resolving small-scale structures is relatively poor. In contrast, the PGNN, which incorporates physical information, achieves more desirable results in reconstructing the turbulent flow field, accurately capturing both large-scale and small-scale features.

The authors posit that the efficacy of incorporating the global pressure field arises from its inherent elliptic nature, as governed by the pressure Poisson equation in the Navier-Stokes (NS) system. Unlike parabolic or hyperbolic equations—which characterize velocity evolution through localized dependencies (e.g., viscous diffusion or convective transport)—elliptic systems require global interdependence, meaning each point in the pressure field is influenced by all other points simultaneously. Consequently, integrating the pressure field into the neural network (NN) inputs provides a mechanism to encode these long-range correlations directly. In contrast, models relying solely on spatial coordinates to map velocity or other flow quantities inherently capture only local relationships, lacking the ability to resolve the non-local interactions critical to pressure-dominated phenomena. By leveraging the elliptic structure of pressure, the NN gains access to the global physical constraints of the system, enabling a more accurate and physically consistent representation of the turbulent field.

CONCLUSIONS

In this study, we proposed a data-driven modeling framework based on Physics-Guided Neural Networks (PGNNs) for the super-resolution reconstruction of turbulent channel flow from low-resolution flow fields. By leveraging the elliptic nature of the pressure equation in incompressible flows and incorporating global pressure data as additional input features, our framework effectively integrates physical principles with machine learning to enhance the accuracy and robustness of super-resolution reconstruction.

The high-fidelity dataset generated through LES provided a solid foundation for training the neural network models. The comparison between the purely data-driven neural network and the proposed PGNN demonstrated that incorporating physical knowledge significantly improves the reconstruction accuracy, especially in capturing small-scale turbulent structures. The PGNN model was able to produce high-resolution flow fields that closely resembled the ground truth obtained from CFD simulations, thereby validating the effectiveness of our approach.

This work highlights the importance of integrating physical insights into machine learning models for complex fluid dynamics problems. The proposed framework not only reduces the computational burden associated with high-resolution CFD simulations but also enhances the generalizability and reliability of super-resolution reconstruction in turbulent flows. Future work may focus on extending this framework to more complex flow configurations, exploring additional physical constraints, and further optimizing the neural network architecture to improve performance and efficiency.

ACKNOWLEDGEMENT

This work is supported by the National Natural Science Foundation of China (52131102), to which the authors are most grateful.

REFERENCES

Bi, X., Liu, A., Fan, Y., Yu, C., Zhang, Z., 2022. FlowSRNet: A multi-scale integration network for super-resolution reconstruction of fluid flows. Physics of Fluids 34, 127104.

Fukami, K., Fukagata, K., Taira, K., 2020. Machine-learning-based spatio-temporal super resolution reconstruction of turbulent flows. Journal of Fluid Mechanics 909, A9.

Fukami, K., Fukagata, K., Taira, K., 2019. Super-resolution reconstruction of turbulent flows with machine learning. Journal of Fluid Mechanics 870, 106–120. https://doi.org/10.1017/jfm.2019.238

Li, B., Ge, M., Li, X., Liu, Y., 2024. A physics-guided machine learning framework for real-time dynamic wake prediction of wind turbines. Physics of Fluids 36, 035143. https://doi.org/10.1063/5.0194764

Liu, B., Tang, J., Huang, H., Lu, X.-Y., 2020. Deep learning methods for super-resolution reconstruction of turbulent flows. Physics of Fluids 32, 025105. https://doi.org/10.1063/1.5140772

Nicoud, F., Ducros, F., 1999. Subgrid-scale stress modelling based on the square of the velocity gradient tensor. Flow Turbul. Combust. 62, 183–200. https://doi.org/10.1023/A:1009995426001

Raissi, M., Perdikaris, P., Karniadakis, G.E., 2019. Physics-informed neural networks: A deep learning framework for solving forward and inverse problems involving nonlinear partial differential equations. Journal of Computational Physics 378, 686–707. https://doi.org/10.1016/j.jcp.2018.10.045

Yousif, M.Z., Yu, L., Lim, H., 2022. Physics-guided deep learning for generating turbulent inflow conditions. Journal of Fluid Mechanics 936, A21.